RESEARCH ARTICLE | MARCH 15 2023

Development of a thermo-pressure acoustic model and its application in modeling three-dimensional acoustofluidic systems **⊘**

Pradipta Kr. Das ; Venkat R. Bhethanabotla ■



Physics of Fluids 35, 036115 (2023) https://doi.org/10.1063/5.0140656





CrossMark

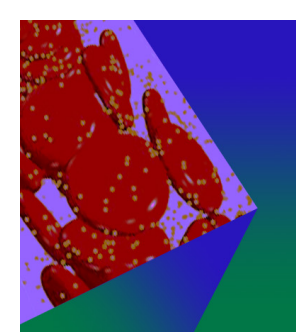
Articles You May Be Interested In

Acoustothermal phase change and acoustically driven atomization for cold liquid microthrusters Appl. Phys. Lett. (January 2023)

Theory of pressure acoustics with thermoviscous boundary layers and streaming in elastic cavities *J Acoust Soc Am* (May 2021)

Acoustothermal heating in surface acoustic wave driven microchannel flow

Physics of Fluids (October 2019)



Physics of Fluids

Special Topic: Flow and Forensics

Submit Today!





Development of a thermo-pressure acoustic model and its application in modeling three-dimensional acoustofluidic systems

Cite as: Phys. Fluids **35**, 036115 (2023); doi: 10.1063/5.0140656 Submitted: 29 December 2022 · Accepted: 22 February 2023 · Published Online: 15 March 2023







Pradipta Kr. Das (D) and Venkat R. Bhethanabotla (D)

AFFILIATIONS

Department of Chemical, Biological, and Materials Engineering, University of South Florida, Tampa, Florida 33620-5350, USA

^{a)}Author to whom correspondence should be addressed: bhethana@usf.edu

ABSTRACT

Theoretical modeling of acoustofluidic systems faces extreme challenges as the thickness of the thermoviscous boundary layer is very small compared to the microscale fluid dimensions. The classical pressure acoustic model overcomes these difficulties and is extensively used in simulating three-dimensional (3D) or large two-dimensional (2D) acoustofluidic systems. However, this model cannot be applied to thermoviscous acoustofluidics, as it does not consider energy conservation. Modeling thermoviscous acoustofluidic systems is, therefore, difficult and restricted to small 2D systems only. Here, we have developed a thermo-pressure acoustic model that can effectively simulate thermoviscous acoustofluidic systems. The model has been validated with the full model by performing numerical simulations for a small 2D acoustofluidic system for which capturing the acoustic boundary layer effect is feasible using the full model. After successful validation, we demonstrate that the thermo-pressure acoustic model can also be applied to studying 3D acoustofluidic systems.

Published under an exclusive license by AIP Publishing. https://doi.org/10.1063/5.0140656

I. INTRODUCTION

Acoustofluidic devices are gaining significant attention over the past few decades due to their potential applications in particle manipulations, ¹⁻⁴ cell sorting, ⁵⁻⁹ cell trapping, ¹⁰⁻¹³ biosensing, ¹⁴⁻¹⁸ and nonspecific binding removal¹⁹⁻²¹ Hence, both theoretical and experimental understanding of the acoustofluidic phenomena is extremely important for designing efficient acoustofluidic devices. However, the theoretical modeling of acoustofluidic systems faces serious challenges due to two factors. First, the complex interaction of acoustics and fluids causes flow fields that indicate the presence of a fast-oscillating flow and a mean slow flow (acoustic streaming) corresponding to two distinct timescales: the fast timescale, often characterized by the acoustic time period, is associated with the oscillatory flow, and the slow timescale, which is several order magnitudes larger than the fast timescale, is associated with acoustic streaming. 22,23 For fluids interacting with an acoustic wave having an angular oscillation frequency ω , the fast timescale (t') can be characterized by ω^{-1} . On the contrary, the slow timescale (τ) can be expressed as $\tau = \varepsilon t'$ leading to $\partial_{t'} = \varepsilon \partial_{\tau}$, where ε is a smallness parameter, such as the acoustic Mach number, which is much smaller than one (i.e. $\varepsilon \ll 1$). Second, in most of the acoustofluidic devices, the acoustic boundary layer thickness is much smaller than the fluid domain, and hence, it is extremely difficult to resolve the boundary layer while solving numerically. To give an overview, acoustofluidic devices are usually operated at 1–100 MHz frequencies for which the thickness of the acoustic boundary layer lies within 0.05–0.5 μ m and it is much smaller than the typical dimensions of the devices (\sim 100–500 μ m). Due to such differences, many times, typical computational capability cannot allow the modeling of 3D or even large 2D fluid domains. In this context, the pressure acoustic model has been developed and it quite effectively handles the acoustofluidic problems. In the classical pressure acoustic theory, the acoustic boundary layer is neglected due to its smallness in compared to the fluid domain. Consequently, it shifts the resonance frequency and often miscalculates the viscous damping. Realizing that, a pressure acoustic model has been recently developed²⁴ that incorporates the boundary layer effects.

In a similar fashion, for thermoviscous acoustofluidic scenarios where the thermal effect cannot be neglected, there is a need for an equivalent pressure acoustic model. Previous studies^{25–28} have shown that acoustic streaming can be significantly altered by imposing background temperature gradients. For instance, Fand and Kaye²⁵ experimentally studied the acoustic streaming near a horizontal heated cylinder and demonstrated that a new type of thermoacoustic streaming consisting of two vortices above the cylinder was generated due to the thermal effect. On the contrary, Michel and Chini²⁶ showed that a

thermally stratified fluid can cause strong baroclinic streaming under the actuation of acoustic waves. Nabavi et al.27 performed an experimental study and illustrated that thermal gradient can significantly affect the acoustic streaming and a sufficient temperature gradient can break the symmetry. Recently, Qiu et al.²⁸ demonstrated that a strong thermoacoustic streaming, having velocity amplitude ~100 times higher than Rayleigh streaming, can be realized in microscale with a temperature gradient as low as 10 K/mm. Thermoacoustic streaming also enhances heat transfer at microscale. Several previous studies²⁹ have analyzed the influence of acoustic streaming on heat transfer. For example, Lin and Farouk³¹ studied the heat transfer characteristics in a closed enclosure with differentially heated walls and concluded that the presence of acoustic streaming significantly improves heat transfer. Other than these studies, it is already established that acoustic-fluid interactions can generate heat inside the fluid and this phenomenon is known as acoustothermal heating.35-45 Kondoh et al.35 showed for the first time that the interaction of surface acoustic wave (SAW) with a water thin film can cause sufficient temperature rise, and the temperature rise can directly be controlled by the applied SAW voltage. Later, in a series of studies,^{36–38} they have shown the effect of duty factor, applied voltage, and liquid viscosity on the acoustothermal heating. Roux-Marchand et al. 45 examined the temperature uniformity in the acoustothermal droplet heating by varying droplet volume, SAW frequency, and SAW power and proposed device structures for an efficient temperature distribution. It is important to note here that most of the acoustothermal heating studies are experimental in nature as theoretical modeling of such systems is extremely challenging and requires significant computational resources. With modern-day computers, only small two-dimensional acoustothermal systems can be numerically solved⁴³ and it is practically impossible to solve threedimensional systems.

To alleviate this situation, in this work, we have developed a thermo-pressure acoustic model that can handle issues related to the length scales associated with the boundary layer and the fluid domain and be effectively used for modeling thermoviscous acoustofluidic systems. We have adopted a perturbative approach to separate the fast and slow timescales and provided a model that can effectively govern the acoustic fields. The model has been validated with the full model for a small two-dimensional fluid domain and extended for three-dimensional systems.

II. BASIC THEORY

A. Governing equations

For our model development, we focused on the fluid domain only and represent the fluid–solid vibrating boundary by an oscillating displacement field. We consider that the fluid domain is filled with a compressible Newtonian thermoviscous fluid, and its density, shear viscosity, bulk viscosity, thermal conductivity, heat capacity, isobaric thermal expansion coefficient, and isothermal compressibility are denoted by ρ , μ , μ , k, k, c, ρ , α , and κ , respectively. Note here that the isothermal compressibility, κ , is related to isobaric compressibility, κ , $\frac{1}{\rho c_0^{-2}}$ as κ , where c0 and γ are the sonic speed and the heat capacity ratio of the fluid, respectively. The governing equations for the thermoviscous fluid are given by

$$\partial_t \rho + \nabla \cdot (\rho \mathbf{v}) = 0, \tag{1}$$

$$\partial_t(\rho \mathbf{v}) = \nabla \cdot [\mathbf{\sigma} - p\mathbf{I} - \rho \mathbf{v}\mathbf{v}], \tag{2}$$

$$\partial_t \left(\rho E + \frac{1}{2} \rho v^2 \right) = \nabla \cdot \left[\mathbf{v} \cdot \mathbf{\sigma} - p \mathbf{v} + k_{th} \nabla T - \rho \left(E + \frac{1}{2} v^2 \right) \mathbf{v} \right]. \tag{3}$$

In the above, p, T, and E are pressure, temperature, and energy of the fluid, respectively. The velocity can be expressed in terms of its components as $\mathbf{v} = v_x \mathbf{e}_x + v_y \mathbf{e}_y + v_z \mathbf{e}_z$, where v_i and \mathbf{e}_i denote the velocity component and the unit vector along the i-direction. The shear stress is given by $\mathbf{\sigma} = \mu [\nabla \mathbf{v} + (\nabla \mathbf{v})^T] + (\mu_b - \frac{2}{3}\mu)[\nabla \cdot \mathbf{v}]\mathbf{I}$ and $v^2 = |\mathbf{v}|^2$. We assume that the vibrating boundary has temperature T_b , and its displacement field is given by $\mathbf{u}_b = \mathbf{u}_{b0}e^{i\omega t}$, where $\omega = 2\pi c_0/\lambda$ is the angular frequency of the oscillation and λ is the wavelength. The velocity at the vibrating boundary can be obtained from the displacement field as $\mathbf{v}_b = \frac{\partial \mathbf{u}_b}{\partial t}$.

B. Separation of timescales

One of the primary difficulties in modeling the acoustofluidic systems is the presence of the multiple timescales associated with the fast-oscillating flow and the acoustic streaming. We use the regular perturbation technique to separate the timescales, and we express the fluid response to the imposed acoustic wave as summation of three components: hydrostatic, acoustic, and mean components. Using the perturbation method, ⁴⁶ we can express each flow and temperature variable in terms of these three components as

$$g = g_0 + \varepsilon g_1 + \varepsilon^2 g_2 + O(\varepsilon^3), \tag{4}$$

where ε is a smallness parameter, indicative of the acoustic Mach number, which is the ratio of the acoustic velocity amplitude and the sonic speed, and in typical acoustofluidics, this number is extremely small⁴⁷ (i.e., $\varepsilon \ll 1$). Here, g represents ρ , p, T, \mathbf{v} , and E. Note here, we assume that the fluid is at rest before the acoustic excitations and, hence, $\mathbf{v}_0 = \mathbf{0}$. We further denote $\tilde{g}_1 = \varepsilon g_1$ and $\bar{g} = \varepsilon^2 g_2$. The thermophysical properties of the fluid depend on the temperature and, therefore, can be expressed in terms of the three components as

$$\mu = \mu_0 + \varepsilon \mu_1 + \varepsilon^2 \mu_2 + O(\varepsilon^3), \tag{5}$$

where
$$\varepsilon \mu_1 \equiv \tilde{\mu}_1 = \left(\frac{d\mu}{dT}\right)_{T=T_0} \tilde{T}_1$$
 and $\varepsilon^2 \mu_2 = \bar{\mu}_2 = \left(\frac{d\mu}{dT}\right)_{T=T_0} \bar{T}_2 + \frac{1}{2} \left(\frac{\partial^2 \mu}{\partial T^2}\right)_{T=T_0} \tilde{T}_1^2$. We can obtain similar expressions for μ_b , k_{th} , c_p , α_p , and κ_T . Substituting Eqs. (4) and (5) into the governing Eqs. (1)–(3) and collecting the similar order terms, we obtain the equations governing the hydrostatics, oscillatory flow, and hydrodynamics of the fluid system.

C. Fluid hydrostatics

Zeroth-order, i.e., $O(\varepsilon^0)$, equations describe the fluid hydrostatics and are given by

$$\partial_t \rho_0 = 0, \tag{6}$$

$$\nabla p_0 = 0, \tag{7}$$

$$\nabla \cdot (k_{th0} \nabla T_0) = 0. \tag{8}$$

Note here that the zeroth-order equations have trivial solutions, which indicate that before the acoustic actuation, there are uniform pressure and temperature distributions inside the fluid and density, ρ_0 , is time invariant.

D. Acoustic fields

First-order [i.e., $O(\varepsilon^1)$] equations describe the oscillatory flow and temperature fields and are given by

$$\partial_t \tilde{\rho}_1 + \rho_0 \nabla \cdot \tilde{\mathbf{v}}_1 = 0, \tag{9}$$

$$\rho_0 \partial_t \tilde{\mathbf{v}}_1 = \nabla \cdot \left[\tilde{\mathbf{\sigma}}_1 - \tilde{p}_1 \mathbf{I} \right], \tag{10}$$

$$\rho_0 \partial_t \tilde{E}_1 + E_0 \partial_t \tilde{\rho}_1 = \nabla \cdot \left[-p_0 \tilde{\mathbf{v}}_1 + k_{th0} \nabla \tilde{T}_1 - E_0 \rho_0 \tilde{\mathbf{v}}_1 \right], \tag{11}$$

where $\tilde{\mathbf{\sigma}}_1 = \mu_0 [\nabla \mathbf{v}_1 + (\nabla \mathbf{v}_1)^T] + (\mu_{b0} - \frac{2}{3}\mu_0) [\nabla \cdot \mathbf{v}_1] \mathbf{I}$. In the above equations, we use following constitutive relationships, expressing $\tilde{\rho}_1$ and \tilde{E}_1 in terms of \tilde{p}_1 and \tilde{T}_1 as

$$d\tilde{\rho}_1 = \rho_0 \left(\kappa_{T0} d\tilde{p}_1 - \alpha_{p0} d\tilde{T}_1 \right) \tag{12}$$

and

$$\rho_0 \tilde{E}_1 = (c_{p0}\rho_0 - \alpha_{p0}p_0)\tilde{T}_1 + (\kappa_{T0}p_0 - \alpha_{p0}T_0)\tilde{p}_1$$
 (13)

and simplified further resulting the following equations:

$$\alpha_{p0}\partial_t \tilde{T}_1 - \kappa_{T0}\partial_t \tilde{p}_1 = \nabla.\tilde{\mathbf{v}}_1, \tag{14}$$

$$\rho_0 \partial_t \tilde{\mathbf{v}}_1 = \mu_0 \nabla^2 \tilde{\mathbf{v}}_1 + \beta \mu_0 \nabla (\nabla \cdot \tilde{\mathbf{v}}_1) - \nabla \tilde{p}_1, \tag{15}$$

$$\rho_0 c_{p0} \partial_t \tilde{T}_1 - \alpha_{p0} T_0 \partial_t \tilde{p}_1 = k_{th0} \nabla^2 \tilde{T}_1, \tag{16}$$

where $\beta = \left(\frac{1}{3} + \frac{\mu_{b0}}{\mu_0}\right)$.

E. Mean flow and temperature fields

Second-order equations [i.e., $O(\varepsilon^2)$] describe the hydrodynamics of the fluid system and are given by

$$\partial_t \bar{\rho}_2 + \rho_0 \nabla \cdot \bar{\mathbf{v}}_2 + \nabla \cdot (\tilde{\rho}_1 \tilde{\mathbf{v}}_1) = 0, \tag{17}$$

$$\rho_0 \partial_t \bar{\mathbf{v}}_2 + \partial_t (\tilde{\rho}_1 \tilde{\mathbf{v}}_1) = \nabla \cdot [\bar{\mathbf{\sigma}}_2 - \bar{p}_2 \mathbf{I} - \rho_0 \tilde{\mathbf{v}}_1 \tilde{\mathbf{v}}_1], \tag{18}$$

$$\partial_{t} \left(\rho_{0} \bar{E}_{2} + \tilde{\rho}_{1} \tilde{E}_{1} + \bar{\rho}_{2} E_{0} + \frac{1}{2} \rho_{0} \tilde{\mathbf{v}}_{1}^{2} \right)$$

$$= \nabla \cdot \left[\tilde{\mathbf{v}}_{1} \cdot \tilde{\mathbf{\sigma}}_{1} - \tilde{p}_{1} \tilde{\mathbf{v}}_{1} - p_{0} \bar{\mathbf{v}}_{2} + \tilde{k}_{th1} \nabla \tilde{T}_{1} + k_{th0} \nabla \bar{T}_{2} - \rho_{0} E_{0} \bar{\mathbf{v}}_{2} - \rho_{0} \tilde{E}_{1} \tilde{\mathbf{v}}_{1} - \tilde{\rho}_{1} E_{0} \tilde{\mathbf{v}}_{1} \right], \tag{19}$$

where $\bar{\sigma}_2 = \mu_0 [\nabla \bar{\mathbf{v}}_2 + (\nabla \bar{\mathbf{v}}_2)^T] + \left(\mu_{b0} - \frac{2}{3}\,\mu_0\right) [\nabla \cdot \bar{\mathbf{v}}_2] \mathbf{I} + \tilde{\mu}_1 [\nabla \tilde{\mathbf{v}}_1 + (\nabla \tilde{\mathbf{v}}_1)^T] + \left(\tilde{\mu}_{b1} - \frac{2}{3}\,\tilde{\mu}_1\right) [\nabla \cdot \tilde{\mathbf{v}}_1] \mathbf{I}$. We need to express these equations in the time-averaged form and solve them for a steady state solution. We set all time derivative to zero and performed a time-averaging over oscillation time period $\Omega = \frac{2\pi}{\omega}$ as

$$\langle g(x, y, t) \rangle = \frac{1}{\Omega} \int_{1}^{t+\Omega} g(x, y, t) dt,$$
 (20)

where $\langle\cdot\rangle$ denotes the time-averaged components. The time-averaging of the product of two oscillatory components, \tilde{g}_1 and \tilde{f}_1 , can be calculated as

$$\langle \tilde{g}_1(x, y, t) \tilde{f}_1(x, y, t) \rangle = \frac{1}{2} \text{Re} \left[\tilde{g}_1^*(x, y, 0) \tilde{f}_1(x, y, 0) \right].$$
 (21)

Here, Re[·] denotes the real component and asterisk (*) indicates the complex conjugate. Using Eqs. (14) and (18), we have simplified

Eq. (19) and the final form of equations governing the mean flow and temperature fields of the fluid at the steady state is given by

$$\rho_0 \nabla \cdot \langle \bar{\mathbf{v}}_2 \rangle + \nabla \cdot \langle \tilde{\rho}_1 \tilde{\mathbf{v}}_1 \rangle = 0, \tag{22}$$

$$\nabla \cdot \left[\langle \bar{\mathbf{\sigma}}_2 \rangle - \langle \bar{p}_2 \rangle \mathbf{I} - \rho_0 \langle \tilde{\mathbf{v}}_1 \tilde{\mathbf{v}}_1 \rangle \right] = 0, \tag{23}$$

$$\nabla \cdot \left[\langle \tilde{\mathbf{v}}_1 \cdot \tilde{\sigma}_1 \rangle - (1 - \alpha_p T_0) \langle \tilde{p}_1 \tilde{\mathbf{v}}_1 \rangle + \langle \tilde{k}_{th1} \nabla \tilde{T}_1 \rangle \right. \\ \left. + k_{th0} \nabla \langle \bar{T}_2 \rangle + \langle \tilde{k}_{th1} \nabla \tilde{T}_1 \rangle - \rho_0 c_p \langle \tilde{T}_1 \tilde{\mathbf{v}}_1 \rangle \right] = 0.$$
 (24)

III. THERMO-PRESSURE ACOUSTIC MODEL

In this section, we develop a thermo-pressure acoustic model that can effectively govern the acoustic fields. To do this, we first differentiate Eq. (15) w.r.t. time, eliminate the acoustic pressure using Eq. (14), and seek harmonic solutions in the form of $\tilde{g}_1 = \hat{g}_1 e^{i\omega t}$ (therefore, replace ∂_t with $i\omega$) to obtain

$$-\rho_0 \tilde{\mathbf{v}}_1 \omega^2 = \frac{1}{\kappa_{T0}} \nabla \left(\nabla \cdot \tilde{\mathbf{v}}_1 - i \omega \alpha_{p0} \tilde{T}_1 \right) + i \omega \mu_0 \nabla^2 \tilde{\mathbf{v}}_1$$
$$+ i \omega \beta \mu_0 \nabla (\nabla \cdot \tilde{\mathbf{v}}_1). \tag{25}$$

Using classical vector identity $\nabla(\nabla \cdot \tilde{\mathbf{v}}_1) = \nabla^2 \tilde{\mathbf{v}}_1 + \nabla \times \nabla \times \tilde{\mathbf{v}}_1$, Eq. (25) can be simplified to

$$\nabla(\nabla \cdot \tilde{\mathbf{v}}_1) - \frac{k_c^2}{k_s^2} \nabla \times \nabla \times \tilde{\mathbf{v}}_1 + k_c^2 \tilde{\mathbf{v}}_1 - \frac{ik_c^2 \alpha_{p0}}{\omega \rho_0 \kappa_{T0}} \nabla \tilde{T}_1 = 0, \quad (26)$$

where $k_c = \frac{\omega^2 \rho_0 \kappa_{T0}}{1 + i\omega \kappa_{T0} \mu_0 (1 + \beta)}$ is the compressional wave number, $k_s = \frac{1 - i}{\delta_s}$ is the shear wave number, and $\delta_s = \sqrt{\frac{2\mu_0}{\omega \rho_0}}$ is the thickness of the Stokes layer. We next use the standard Helmholtz decomposition of the acoustic velocity field, $\tilde{\mathbf{v}}_1 = \nabla \tilde{\phi} + \nabla \times \tilde{\psi}$, where $\tilde{\phi}$ and $\tilde{\psi}$ are the scalar and the vector potentials, respectively, and obtain the following set of equations:

$$\nabla^2 \tilde{\mathbf{v}}_{1\delta} + k_s^2 \tilde{\mathbf{v}}_{1\delta} + \frac{k_s^2 \alpha_{p0}}{i\omega \rho_0 \kappa_{T0}} \nabla \tilde{T}_{1\delta} = 0, \tag{27a}$$

$$\nabla(\nabla \cdot \tilde{\mathbf{v}}_{1s}) + k_c^2 \tilde{\mathbf{v}}_{1s} - \frac{ik_c^2 \alpha_{p0}}{\omega \rho_0 \kappa_{T0}} \nabla \tilde{T}_{1s} = 0.$$
 (27b)

In the above, $\tilde{\mathbf{v}}_{1s} = \nabla \tilde{\varphi}$ and $\tilde{\mathbf{v}}_{1\delta} = \nabla \times \tilde{\mathbf{\psi}}$ are the acoustic velocity fields associated with the scalar and the vector potentials, respectively. Please note that $\tilde{\mathbf{v}}_{1\delta}$ basically dictates the acoustic velocity field inside the Stokes layer where vorticity is non-zero and $\tilde{\mathbf{v}}_{1s}$ indicates the bulk acoustic velocity field. The associated temperature fields are denoted as $\tilde{T}_{1\delta}$ and \tilde{T}_{1s} , respectively, such that $\tilde{T}_1 = \tilde{T}_{1s} + \tilde{T}_{1\delta}$. Similarly, the acoustic pressure fields due to the scalar and the vector velocity potentials are denoted as \tilde{p}_{1s} and $\tilde{p}_{1\delta}$, respectively, where $\tilde{p}_1 = \tilde{p}_{1s} + \tilde{p}_{1\delta}$. To solve Eq. (27a), we consider the boundary layer thickness δ_s to be very small compared to the wavelength scale $k^{-1} = c_0/\omega$, which is true for almost all the acoustofluidic systems. We used the scaling analysis similar to our previous study⁴⁷ and obtained the governing equation for $\tilde{\mathbf{v}}_{1\delta}$ inside the Stokes layer as

$$\frac{\partial^2 \tilde{\mathbf{v}}_{1\delta}}{\partial y^2} \approx -k_s^2 \tilde{\mathbf{v}}_{1\delta},\tag{28}$$

where *y* is the coordinate normal to the vibrating boundary and the acoustic velocity field inside the boundary layer can be calculated as

$$\tilde{\mathbf{v}}_{1\delta} = \mathbf{v}_b e^{-ik_s y}.\tag{29}$$

In a similar way, the energy conservation equation in the Stokes layer can be derived from Eq. (16). We expressed it as follows by putting $\partial_t \rightarrow i\omega$:

$$i\omega \left(\rho_0 c_{p0} \tilde{T}_{1\delta} - \alpha_{p0} T_0 \tilde{p}_{1\delta}\right) = k_{th0} \nabla^2 \tilde{T}_{1\delta}. \tag{30}$$

Note that, following our previous study, 47 the variation of the acoustic pressure inside the Stokes layer can safely be neglected ($\tilde{p}_{1\delta}\approx 0$) leading to an expression for $\tilde{T}_{1\delta}$ as

$$\frac{\partial^2 \tilde{T}_{1\delta}}{\partial v^2} \approx -k_t^2 \tilde{T}_{1\delta}.\tag{31}$$

The solution of the equation is given by

$$\tilde{T}_{1\delta} = \tilde{T}_{b1} e^{-ik_t y}.$$
(32)

In the above, $\tilde{T}_{b1} = T_b - T_0$ is the acoustic temperature at the vibrating boundary, $k_t = \frac{1-i}{\delta_t}$ is the thermal wave number, and $\delta_t = \sqrt{2k_{th0}/\omega\rho_0c_{p0}}$ is the thickness of the thermal boundary layer. Utilizing Eq. (14), Eq. (27b) can be further simplified to

$$\tilde{\mathbf{v}}_{1s} = \frac{\alpha_{p0}\Gamma_{\nu}}{\omega\kappa_{T0}\rho_{0}}\nabla\tilde{T}_{1s} + \frac{(i-\Gamma_{\nu})}{\omega\rho_{0}}\nabla\tilde{p}_{1s},\tag{33}$$

where $\Gamma_{\nu} = \omega(1+\beta)\mu_0\kappa_{T0}$ is the damping factor associated with the viscous effect. We substitute above expression of $\tilde{\mathbf{v}}_{1s}$ in Eq. (14) and express it in terms of the acoustic pressure and the temperature fields as

$$[1+i\Gamma_{\nu}]\nabla^{2}\tilde{p}_{1s} = \frac{i\Gamma_{\nu}\alpha_{p0}}{\kappa_{T0}}\nabla^{2}\tilde{T}_{1s} + \rho_{0}\omega^{2}\left(\alpha_{p}\tilde{T}_{1s} - \kappa_{T}\tilde{p}_{1s}\right). \tag{34}$$

The associated energy equation becomes

$$i\omega \left(\rho_0 c_{p0} \tilde{T}_{1s} - \alpha_{p0} T_0 \tilde{p}_{1s}\right) = k_{th0} \nabla^2 \tilde{T}_{1s}.$$
 (35)

With these, the acoustic field can be governed by the thermo-pressure acoustic model comprising of Eqs. (34) and (35) in conjunction with Eqs. (29) and (32).

IV. MODEL VALIDATION

In this section, we have implemented the thermo-pressure acoustic model in finite element method based commercial software COMSOL Multiphysics and validated it with the full model. The problem considered for the validation is a two-dimensional PDMS (polydimethylsiloxane) microchannel excited by a standing SAW as schematically shown in Fig. 1(a).

We considered the fluid domain as the computational domain $[Fig.\ 1(b)]$ where bottom boundary has a SAW displacement field defined as

$$\mathbf{u}_b = u_{b0x}\mathbf{e}_x + u_{b0y}\mathbf{e}_y \quad \text{on} \quad S_i, \tag{36}$$

where

$$u_{b0x} = \xi u_{b0} \left[e^{-c_d \left(\frac{W}{2} - x \right)} e^{-ik_x \left(\frac{W}{2} - x \right)} + e^{-c_d \left(\frac{W}{2} + x \right)} e^{ik_x \left(\frac{W}{2} - x \right)} \right] e^{i\omega t}, \quad (37a)$$

$$u_{b0y} = u_{b0} \left[e^{-c_d \left(\frac{W}{2} + x \right)} e^{ik_x \left(\frac{W}{2} - x \right) - i\frac{\pi}{2}} - e^{-c_d \left(\frac{W}{2} - x \right)} e^{-ik_x \left(\frac{W}{2} - x \right) - i\frac{\pi}{2}} \right] e^{i\omega t}, \quad (37b)$$

where c_d is the attenuation coefficient of the SAW displacement field and it is given by $c_d = \frac{\rho_0 c_0}{\rho_{LN} c_{LN} \lambda}$. ρ_{LN} and c_{LN} are the density and the sonic speed of lithium niobate piezoelectric substrate, respectively. k_x is the wave vector of the SAW, and it is given by $k_x = 2\pi/\lambda$. We also assume that the bottom boundary is at ambient temperature T_0 . On other sides, acoustic impedance boundary conditions are specified. The heat loss through the PDMS wall has been taken care of through convective boundary condition and convective heat loss can be prescribed by $\mathbf{n} \cdot (-k_{th} \nabla T) = h_{eff}(T-T_0)$.

The appropriate boundary condition at the bottom boundary, required to solve Eqs. (34) and (35), can be derived from Eq. (33) as

$$\mathbf{n} \cdot \nabla \tilde{p}_1 = \frac{i \Gamma_{\nu} \alpha_{p0} (\mathbf{n} \cdot \nabla \tilde{T}_{1s}) + \rho_0 \kappa_{T0} \omega^2 (\mathbf{n} \cdot \mathbf{u}_b)}{\kappa_{T0} (1 + i \Gamma_{\nu})} \quad \text{on } S_i.$$
 (38)

The acoustic temperature at the bottom boundary is taken as zero, i.e.,

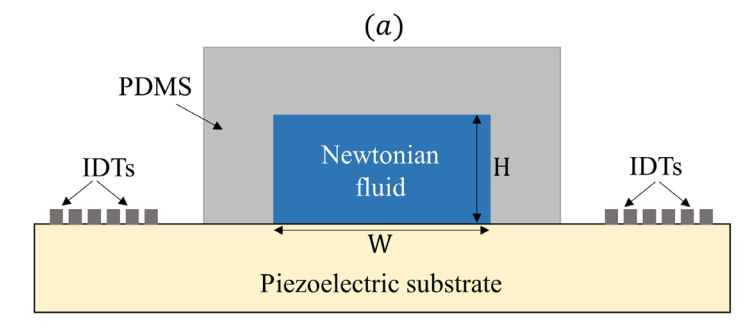
$$\tilde{T}_{1s} = 0 \quad \text{on } S_i. \tag{39}$$

On the other boundaries, the following conditions are used

$$\mathbf{n} \cdot \nabla \tilde{p}_{1s} = -\frac{i\omega \rho_0}{\rho_{m} c_m} \tilde{p}_{1s} \quad \text{on } S_W, \tag{40}$$

$$\mathbf{n} \cdot \left(-k_{th0} \nabla \tilde{T}_{1s} \right) = h_{eff} \tilde{T}_{1s} \quad \text{on } S_W. \tag{41}$$

The boundary conditions used to calculate the acoustic fields for both the thermo-pressure acoustic model and the full model are shown in Table I.



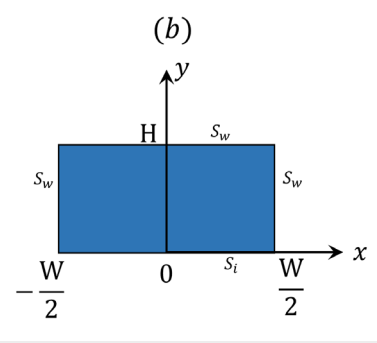


FIG. 1. Schematic diagram showing (a) the physical system of the surface acoustic wave driven PDMS microchannel of width W and height H, filled with Newtonian fluids and (b) the corresponding computational domain along with the associated coordinate system.

TABLE I. The governing equations and the associated boundary conditions for the thermo-pressure acoustic model and the full model for the calculation of acoustic fields

| Properties | Thermo-pressure acoustic model [Eqs. (34) and (35)] | Full model [Eqs. (14)–(16)] |
|----------------------------|--|---|
| At bottom (on S_i) | $\mathbf{n} \cdot \nabla \tilde{p}_{1s} = \frac{i\Gamma_{\nu} \alpha_{p0} (\mathbf{n} \cdot \nabla \tilde{T}_{1s}) + \rho_0 \kappa_{T0} \omega^2 (\mathbf{n} \cdot \mathbf{u}_b)}{\kappa_{T0} (1 + i\Gamma_{\nu})};$ | $	ilde{\mathbf{v}}_1 = \partial_t \mathbf{u}_b$ |
| | ${\tilde T}_{1s}=0$ | ${	ilde T}_1=0$ |
| At other walls (on S_w) | $egin{aligned} \mathbf{n} \cdot abla 	ilde{p}_{1s} &= -rac{i\omega ho_0}{ ho_m c_m} 	ilde{p}_{1s} \ \mathbf{n} \cdot (-k_{th0} abla 	ilde{T}_{1s}) &= h_{eff} 	ilde{T}_{1s} \end{aligned}$ | $egin{aligned} \mathbf{n} \cdot abla 	ilde{p}_1 &= -rac{i\omega ho_0}{ ho_m c_m} 	ilde{p}_1 \ \mathbf{n} \cdot (-k_{th0} abla 	ilde{T}_1) &= h_{eff} 	ilde{T}_1 \end{aligned}$ |
| | $\mathbf{n}\cdot(-k_{th0} abla	ilde{T}_{1s})=h_{e\!f\!f}	ilde{T}_{1s}$ | $\mathbf{n}\cdot(-k_{th0} abla	ilde{T}_1)=h_{eff}	ilde{T}_1$ |
| Closure | $	ilde{\mathbf{v}}_{1s} = rac{lpha_{p0}\Gamma_{ u}}{\omega\kappa_{T0} ho_0} abla 	ilde{T}_{1s} + rac{(i-\Gamma_{ u})}{\omega ho_0} abla 	ilde{p}_1$ | |
| | $egin{array}{l} 	ilde{\mathbf{v}}_{1s} = 	ilde{\mathbf{v}}_{1\delta} & 	ilde{\mathbf{v}}_{1\delta} \ 	ilde{T}_1 = 	ilde{T}_{1s} + 	ilde{T}_{1\delta} \end{array}$ | |
| | 1 10 10 | |
| | ${	ilde p}_1={	ilde p}_{1s}+{	ilde p}_{1\delta}$ | |

The acoustic fields are calculated using the thermo-pressure acoustic model and the full model for the following parameters: $u_{bo} = 1.0 \text{ nm}, \quad \xi = 0.86, \quad W = 160 \,\mu\text{m}, \quad H = 80 \,\mu\text{m}, \quad \lambda = 80 \,\mu\text{m},$ $c_0=1496.7\,\mathrm{m/s}, \mathrm{\ and\ } h_{e\!f\!f}=4.286\,\mathrm{W\,m^{-2}K^{-1}}.$ The thermophysical properties of fluid, PDMS, and lithium niobate, used for the numerical study, are taken same as specified in Table I of our previous study. 43 Figure 2 shows the acoustic pressure (\hat{p}_1) , velocity $(\hat{\mathbf{v}} = \hat{v}_{1x} \mathbf{e}_x)$ $+\widehat{v}_{1y}\mathbf{e}_{y}$), and temperature (T_{1}) fields at time $t=2\pi m$, where m is an integer. These fields are correlated with oscillatory acoustic fields as $\tilde{g}_1 = \hat{g}e^{i\omega t}$ (\tilde{g}_1 represents \tilde{p}_1 , $\tilde{\mathbf{v}}_1$, \tilde{T}_1). Clearly, the thermo-pressure acoustic model results show excellent agreement with the full model as observed from the figure. This, therefore, confirms that the thermopressure acoustic model developed in the present study can essentially capture the physics in governing the acoustic fields in a thermo-viscous acoustofluidic systems. In both the simulations, the mesh independent tests are performed similar to that reported in our previous study. 48 We have observed an extremely reduced solution time while solving the thermo-pressure acoustic model. While it takes 210s to solve the full model on an Intel Core i7-7500U @2.70 GHz processor with 32 GB ram, the computation time of only 9 s is required to solve the thermo-pressure acoustic model, making it ca. 23 times faster.

V. MODELING OF THREE-DIMENSIONAL ACOUSTOFLUIDIC SYSTEMS

After successfully validating the thermo-pressure acoustic model, we have extended our study by simulating three-dimensional acousto-fluidic devices. For that, we consider the standing surface acoustic wave driven PDMS microchannel system of width W and height H, filled with fluid having similar thermophysical properties specified in Sec. IV. The surface acoustic wave is applied to the specific region at the bottom of the microchannel, and the displacement field is given by Eqs. (36) and (37).

A. Acoustic fields

First, we solved the thermo-pressure acoustic model to compute the acoustic fields inside the fluid domain. By exploiting the symmetry around z=0 plane, only one half of the system has been considered for the numerical study. We simulated the microchannel of length L and used perfectly matched layer (PML) of length L_{PML} at the end of the device to absorb all incoming wavefields. The computational domain with the associated coordinate system is schematically shown in Fig. 3. The boundary conditions used to solve the thermo-pressure acoustic model are shown below:

(i) At planar symmetry (z = 0)

$$\mathbf{n} \cdot \nabla \tilde{p}_1 = 0, \tag{42}$$

$$\mathbf{n} \cdot \nabla \tilde{T}_{1s} = 0. \tag{43}$$

(ii) At the side $(x = \pm \frac{W}{2})$ and top (y = H)

$$\mathbf{n} \cdot \nabla \tilde{p}_1 = -\frac{i\omega \rho_0}{\rho_m c_m} \tilde{p}_1,\tag{44}$$

$$\mathbf{n} \cdot \left(-k_{th0} \nabla \tilde{T}_{1s} \right) = h_{eff} \tilde{T}_{1s}. \tag{45}$$

(iii) At the bottom (y = 0),

$$\mathbf{n} \cdot \nabla \tilde{p}_1 = \begin{cases} \frac{i \Gamma_{\nu} \alpha_{p0} \partial_{y} \tilde{T}_{1s} + \rho_0 \kappa_{T0} \omega^2 (\mathbf{n} \cdot \mathbf{u}_b)}{\kappa_{T0} (1 + i \Gamma_{\nu})} & \text{for } 0 \leq z \leq \frac{L}{2}, \\ 0 & \text{for } \frac{L}{2} \leq z \leq \frac{L}{2} + L_{PML}, \end{cases}$$

where $\tilde{u}_{1y} = u_{b0y}$,

(46)

$$\tilde{T}_{1s} = 0. \tag{47}$$

(iv) At outlet $(z = \frac{L}{2} + L_{PML})$

$$\tilde{p}_1 = 0, \tag{48}$$

$$\tilde{T}_{1s} = 0, \tag{49}$$

Please note here that at the vibrating bottom boundary, $T_{b1} = 0$ and $\mathbf{v}_b = \frac{\partial \mathbf{u}_b}{\partial t}$. We calculated the acoustic pressure, temperature, and velocity field for the following parameters: $u_{bo} = 1.0 \text{ nm}$, $\xi = 0.86$,

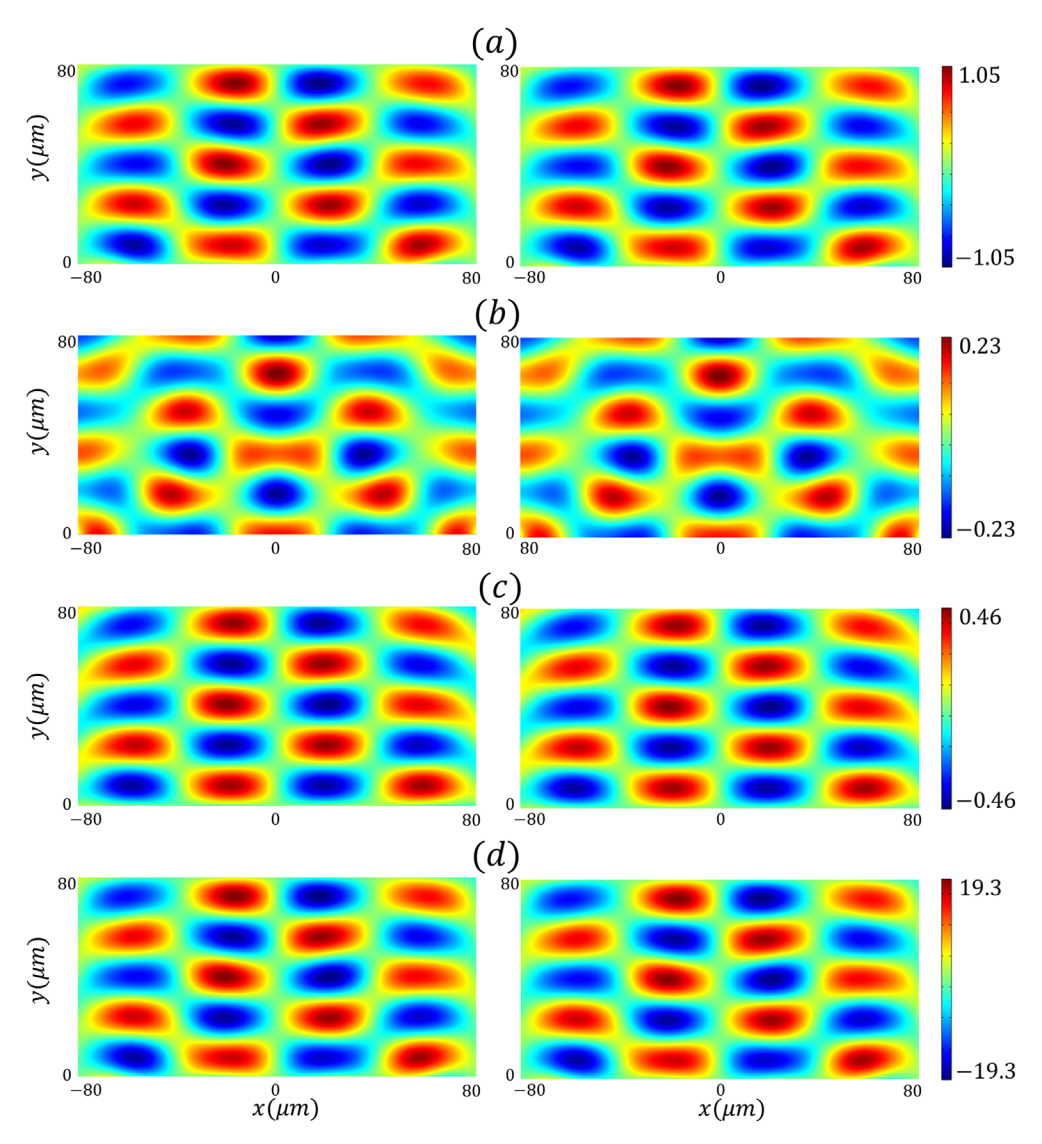


FIG. 2. Comparison of the surface plot of \widehat{p}_1 in MPa (a), \widehat{v}_{1x} in m/s (b), \widehat{v}_{1y} in m/s (c), and \widehat{T}_1 in mK (d) obtained from the solutions of the thermo-pressure acoustic model (left) and the full model (right).

 $\lambda = 80 \ \mu\text{m}$, $W = L = \lambda$, $H = \lambda/4$, $L_{PML} = \lambda/2$, $c_0 = 1496.7 \ \text{m/s}$, and $h_{eff} = 4.286 \ \text{W m}^{-2} \text{K}^{-1}$. We performed the mesh independence test (see the supplementary material), and with the appropriate mesh, the computational time for solving the thermo-pressure acoustic equation is only 1206 s for this 3D system.

Figure 4 shows the acoustic pressure (\widehat{p}_1) , temperature (T_1) , and velocity components $(\widehat{v}_{1x}, \widehat{v}_{1y})$ along z=0, L/4, L/2, and $L/2+L_{PML}/2$ planes for $t=2\pi m$. It is observed that a standing wave is formed in the channel along the x-direction, and it is antisymmetric along the x=0 plane. It is also seen that the acoustic pressure [Fig. 4(a)] and the acoustic temperature [Fig. 4(b)] fields are in the same phase, and their maximum magnitudes are located at planes $\lambda/4$ shifted from the z=0 plane. On contrary, maximum value of both

the acoustic velocity components is located at the z = 0 plane [Figs. 4(c) and 4(d)].

The variation of the acoustic velocity magnitude along the length and the height of the microchannel has also been analyzed. We plot $|\hat{\mathbf{v}}_1|$ along z=0, L/4, L/2, and $L/2+L_{PML}/2$ planes [Fig. 5(a)] and along y=H/4 [Fig. 5(b)], y=H/2 [Fig. 5(c)], and y=3H/4 [Fig. 5(d)] planes. The vector plots of the velocity components on those planes are also shown to illustrate the flow direction. Due to antisymmetric nature of the standing waves across x=0, the oscillatory flow vectors are observed to be in the reverse direction. Another interesting observation is that the flow $(\hat{\mathbf{v}}_{1\delta})$ and the temperature $(\hat{T}_{1\delta})$ fields due to the velocity vector potential are insignificant and can safely be neglected in three-dimensional acoustofluidic devices.

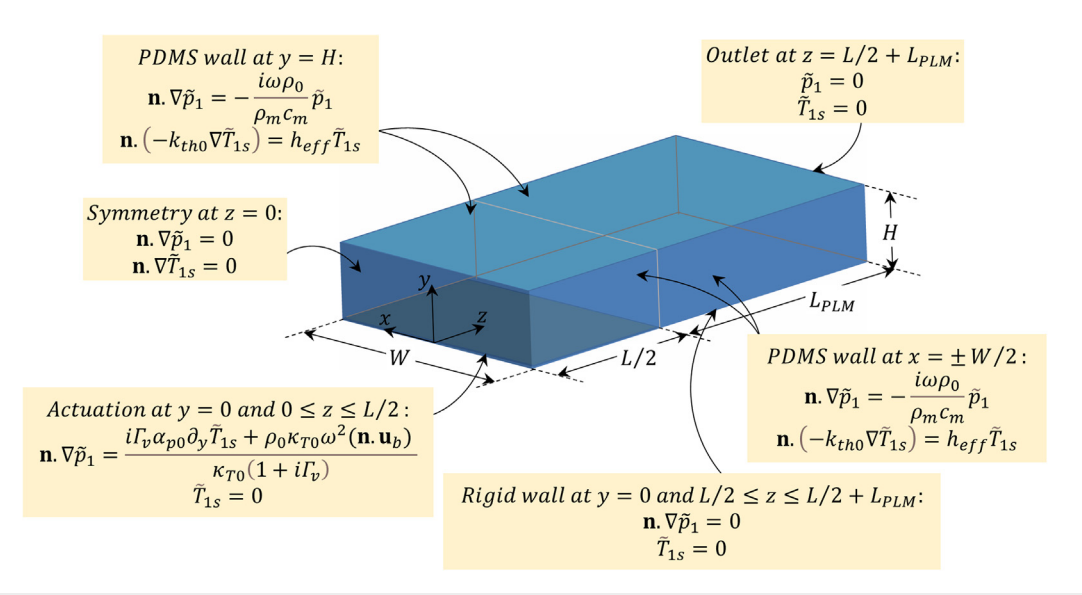


FIG. 3. Computational domain and the associated boundary conditions considered for the surface acoustic wave driven 3D acoustofluidic device.

B. Acoustic streaming and thermal fields

Next, we march forward to calculate the mean flow and the temperature fields governed by Eqs. (22)–(24). Note here that Eqs. (22) and (23) are coupled and can be solved to obtain acoustic streaming fields

inside the microchannel, whereas the acoustothermal field is estimated by solving Eq. (24) only. We used a well established limiting velocity approach⁴⁹ to calculate the acoustic streaming for a three-dimensional acoustofluidic system where the limiting velocities are given by

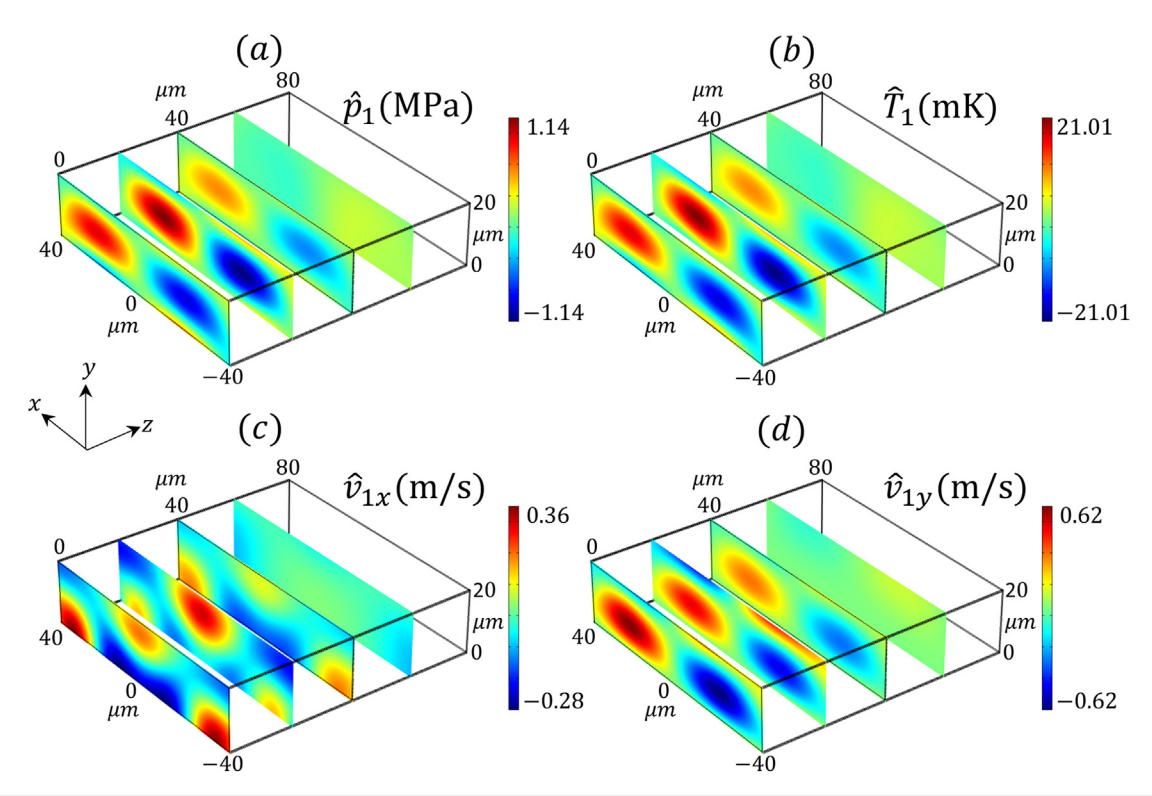


FIG. 4. The variation of the acoustic pressure \widehat{p}_1 (a), temperature \widehat{T}_1 (b), x-component of velocity \widehat{v}_{1x} (c), and y-component velocity \widehat{v}_{1y} (d) along z=0, L/4, L/2, and $L/2+L_{PML}/2$ planes for $t=2\pi m$ in the surface acoustic wave driven three-dimensional microchannel system described in the text.

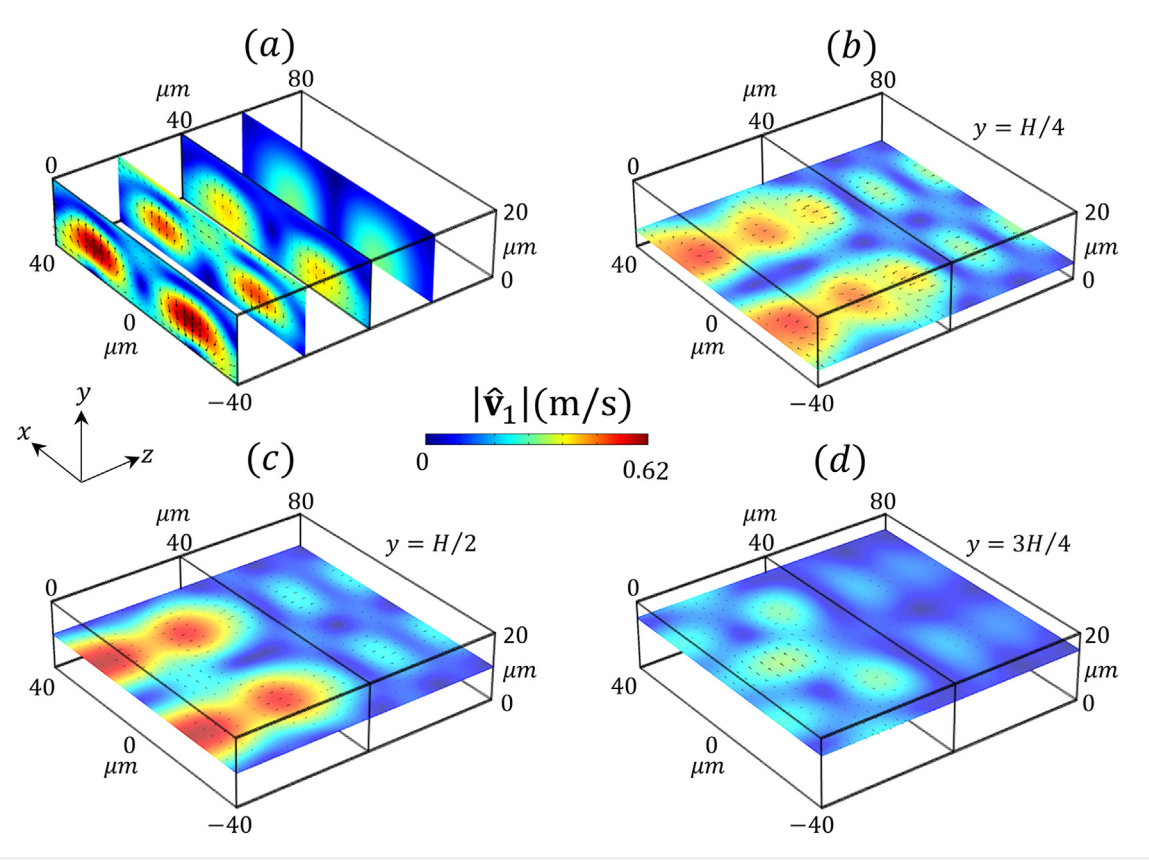


FIG. 5. The variation of the acoustic velocity magnitude $|\bar{\mathbf{v}}_1|$ along z=0, L/4, L/2, and $L/2+L_{PML}/2$ (a), y=H/4(b), y=H/2 (c), and y=3H/4 (d) planes. Black arrows depict the velocity vectors on each plane. Results are shown for the surface acoustic wave driven three-dimensional microchannel system described in the text.

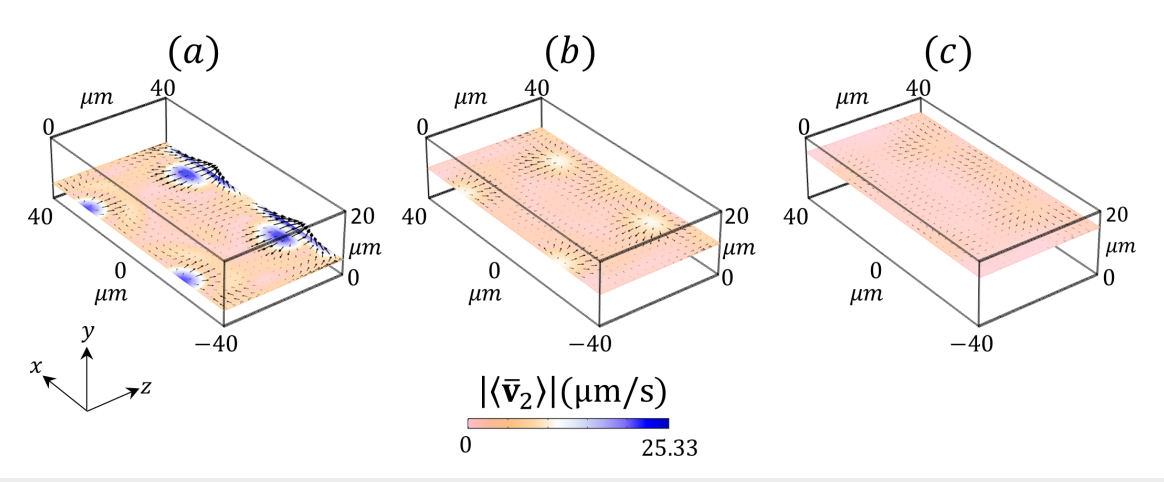


FIG. 6. Color plot of acoustic streaming magnitude along y = H/4 (a), y = H/2 (b), and y = 3H/4 (c) planes. Black arrows show the acoustic streaming vectors on those planes.

$$\bar{v}_{x2L} = -\frac{1}{4\omega} \operatorname{Re} \left\{ \tilde{v}_{x1} \frac{d\tilde{v}_{x1}^*}{dx} + \tilde{v}_{z1} \frac{d\tilde{v}_{x1}^*}{dz} \right. \\ \left. + \tilde{v}_{x1}^* \left[(2+i)\nabla \cdot \tilde{\mathbf{v}}_1 - (2+3i) \frac{d\tilde{v}_{y1}}{dy} \right] \right\}, \tag{50}$$

$$= -\frac{1}{4\omega} \operatorname{Re} \left\{ \tilde{v}_{x1} \frac{d\tilde{v}_{z1}^*}{dx} + \tilde{v}_{z1} \frac{d\tilde{v}_{z1}^*}{dz} + \tilde{v}_{z1} \frac{d\tilde{v}_{z1}^*}{dz} \right\}. \tag{51}$$

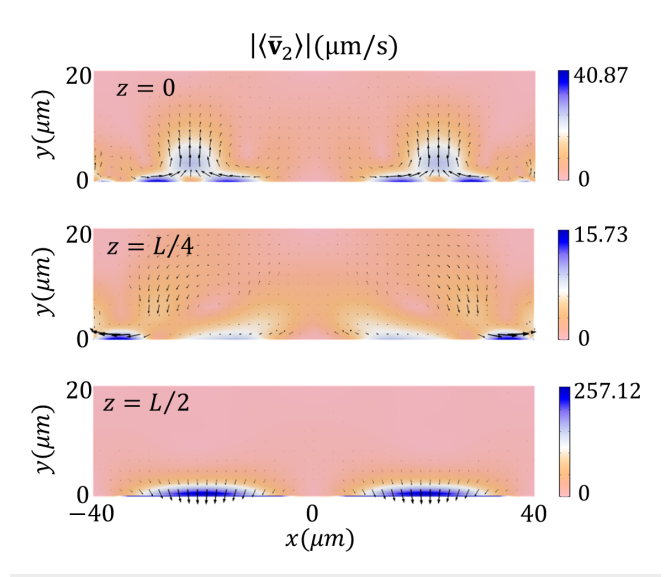


FIG. 7. Color plot of the acoustic streaming magnitude along z=0, z=L/4, and z=L/2 planes. Black arrows show the acoustic streaming vectors on those planes.

In the limiting velocity method, we solved the Stokes equation with no body force and the fluid motion is actuated inside the fluid by the limiting velocities assigned at the bottom boundary (y=0, $0 \le z \le \frac{L}{2}$). In other boundaries, a slip velocity is prescribed. Figure 6 shows the acoustic streaming velocity magnitude along y=H/4 [Fig. 6(a)], y=H/2 [Fig. 6(b)], and y=3H/4 [Fig. 6(c)] planes. We observed that the velocity field is symmetric along x=0 and the maximum velocity magnitude is observed near z=0 and z=L/2. We plot acoustic streaming velocity magnitude along z=0, L/4, and L/2 planes in Fig. 7, and it indicates that with increasing distance from the microchannel bottom, the acoustic streaming fields weaken, ensuring a steep velocity gradient near the vibrating boundary.

To calculate the mean thermal fields, Eq. (24) is solved in conjunction with the following boundary conditions:

- i) At z=0, we used an insulation boundary condition $(\mathbf{n}\cdot\nabla\langle\bar{T}_2\rangle=0).$
- (ii) At $z = L/2 + L_{PML}$ and y = 0 planes, the temperature is same as that of the ambient leading to $\langle \bar{T}_2 \rangle = 0$.
- (iii) At other boundaries, a convective heat loss is prescribed, i.e., $\mathbf{n} \cdot (-k_{th0}\nabla \langle \bar{T}_2 \rangle \langle k_{th1}\nabla \tilde{T}_1 \rangle) = h_{eff} \langle \bar{T}_2 \rangle$.

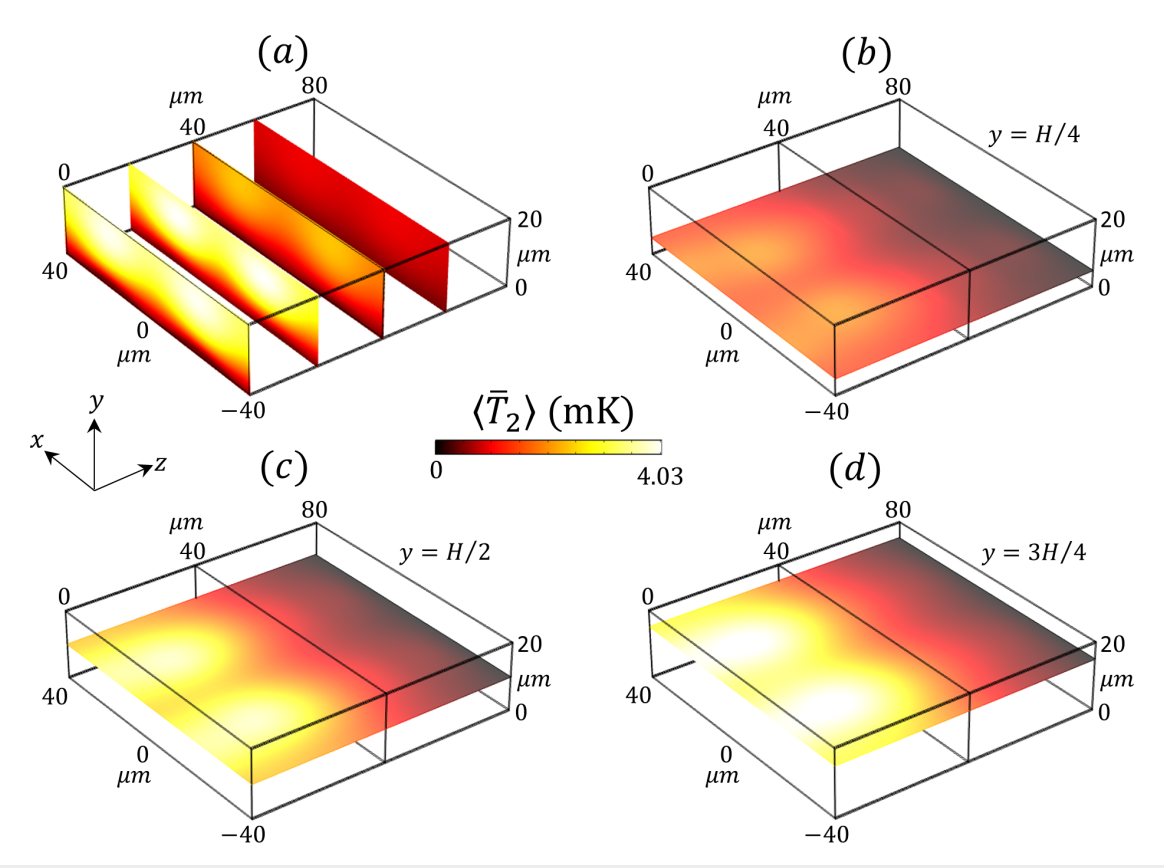


FIG. 8. Color plot of the acoustothermal temperature field along z = 0, L/4, L/2, and $L/2 + L_{PML}/2$ planes (a), y = H/4 (b), y = H/2 (c), and y = 3H/4 (d). Results are shown for the surface acoustic wave driven three-dimensional microchannel system described in the text.

Figure 8 shows the acoustothermal temperature profile on various planes. The temperature profile is observed to be symmetric along the x=0 plane, similar to that observed for the acoustic streaming. We also showed that the maximum temperature is estimated to be 4.03 mK only, and it is observed near the top surface along the z=0 plane.

VI. CONCLUSION

In conclusion, we have developed a thermo-pressure acoustic model to effectively simulate the acoustic fields in thermoviscous acoustofluidic systems. The model assumes that the acoustic boundary layer thickness is very small compared to the acoustic wavelength scale, i.e., $\delta_s \ll k^{-1}$. Please note that such assumptions are true for almost all the acoustofluidic devices unless the fluid is highly viscous or the device is operated at very high frequencies (~GHz).⁴⁷ The model has been validated with the full model for a small twodimensional fluid domain since the full model requires a significant number of fine meshes near the boundary for capturing acoustic boundary layer phenomena. The thermo-pressure acoustic model consumes a less computational memory and calculates the acoustic field extremely rapidly. After successful validation, we have demonstrated the usability of the thermo-pressure acoustic model by simulating a three-dimensional acoustofluidic system, which is otherwise almost impossible to simulate using the full model. The present study also shows that the calculated acoustic fields can be effectively used to model the mean temperature and flow fields.

SUPPLEMENTARY MATERIAL

See the supplementary material for the mesh convergence results, which are used to select the appropriate mesh for carrying out the numerical study for the 3D acoustofluidic system.

ACKNOWLEDGMENTS

This work was funded by the National Science Foundation Grant No. CMI-2108795, which is gratefully acknowledged. Pradipta Kr. Das gratefully acknowledges a University of South Florida Presidential Fellowship.

AUTHOR DECLARATIONS Conflict of Interest

The authors have no conflicts to disclose.

Author Contributions

Pradipta Kr Das: Conceptualization (lead); Formal analysis (lead); Investigation (lead); Methodology (lead); Validation (lead); Writing – original draft (lead). **Venkat R. Bhethanabotla:** Funding acquisition (lead); Resources (lead); Supervision (lead); Writing – review & editing (lead).

DATA AVAILABILITY

The data that support the findings of this study are available within the article and its supplementary material.

REFERENCES

- ¹D. J. Collins, T. Alan, and A. Neild, "Particle separation using virtual deterministic lateral displacement (vDLD)," Lab Chip 14, 1595 (2014).
- ²D. J. Collins, Z. Ma, J. Han, and Y. Ai, "Continuous micro-vortex-based nano-particle manipulation via focused surface acoustic waves," Lab Chip 17, 91 (2017)
- ³S. Li, F. Ma, H. Bachman, C. E. Cameron, X. Zeng, and T. J. Huang, "Acoustofluidic bacteria separation," J. Micromech. Microeng. 27, 015031 (2017)
- ⁴G. Celik Cogal, P. K. Das, S. Li, A. U. Oksuz, and V. R. Bhethanabotla, "Unraveling the autonomous motion of polymer-based catalytic micromotors under chemical–acoustic hybrid power," Adv. NanoBiomed Res. 1, 2000009 (2021).
- ⁵D. Ahmed, A. Ozcelik, N. Bojanala, N. Nama, A. Upadhyay, Y. Chen, W. Hanna-Rose, and T. J. Huang, "Rotational manipulation of single cells and organisms using acoustic waves," Nat. Commun. 7, 11085 (2016).
- ⁶Y. Ai, C. K. Sanders, and B. L. Marrone, "Separation of *Escherichia coli* bacteria from peripheral blood mononuclear cells using standing surface acoustic waves," Anal. Chem. **85**, 9126 (2013).
- ⁷P. Augustsson, C. Magnusson, M. Nordin, H. Lilja, and T. Laurell, "Microfluidic, label-free enrichment of prostate cancer cells in blood based on acoustophoresis," Anal. Chem. **84**, 7954 (2012).
- ⁸T. Franke, S. Braunmüller, L. Schmid, A. Wixforth, and D. A. Weitz, "Surface acoustic wave actuated cell sorting (SAWACS)," Lab Chip 10, 789 (2010).
- ⁹P. Li, Z. Mao, Z. Peng, L. Zhou, Y. Chen, P.-H. Huang, C. I. Truica, J. J. Drabick, W. S. El-Deiry, M. Dao, S. Suresh, and T. J. Huang, "Acoustic separation of circulating tumor cells," Proc. Natl. Acad. Sci. U. S. A. 112, 4970 (2015).
- 10 H. Cong, J. Chen, and H.-P. Ho, "Trapping, sorting and transferring of microparticles and live cells using electric current-induced thermal tweezers," Sens. Actuators B 264, 224 (2018).
- ¹¹M. Evander and J. Nilsson, "Acoustofluidics 20: Applications in acoustic trapping," Lab Chip 12, 4667 (2012).
- ¹²L. Johansson, M. Evander, T. Lilliehorn, M. Almqvist, J. Nilsson, T. Laurell, and S. Johansson, "Temperature and trapping characterization of an acoustic trap with miniaturized integrated transducers – towards in-trap temperature regulation," Ultrasonics 53, 1020 (2013).
- ¹³A. Ozcelik, J. Rufo, F. Guo, Y. Gu, P. Li, J. Lata, and T. J. Huang, "Acoustic tweezers for the life sciences," Nat. Methods 15, 1021 (2018).
- ¹⁴C. T. Chuang, R. M. White, and J. J. Bernstein, "A thin-membrane surface-acoustic-wave vapor-sensing device," IEEE Electron. Device Lett. 3, 145 (1982).
- 15S. Cular, V. R. Bhethanabotla, and D. W. Branch, "P2I-6 vapor discrimination using a hexagonal surface acoustic wave device," in *IEEE Ultrasonics Symposium*, Vancouver, BC, Canada, 2006 (IEEE, Piscataway, NJ, 2006), pp. 1794–1796.
- ¹⁶D. D. Deobagkar, V. Limaye, S. Sinha, and R. D. S. Yadava, "Acoustic wave immunosensing of Escherichia coli in water," Sens. Actuators B 104, 85 (2005).
- ¹⁷C.-T. Feng, C.-J. Cheng, and M. Z. Atashbar, PMMA/64° YX-LiNbO 3 Guided SH-SAW Based Immunosensing System (IEEE, 2011).
- ¹⁸Y. Huang, P. K. Das, and V. R. Bhethanabotla, "Surface acoustic waves in biosensing applications," Sens. Actuators Rep. 3, 100041 (2021).
- ¹⁹G. Celik Cogal, P. K. Das, G. Yurdabak Karaca, V. R. Bhethanabotla, and A. Uygun Oksuz, "Fluorescence detection of miRNA-21 Using Au/Pt bimetallic tubular micromotors driven by chemical and surface acoustic wave forces," ACS Appl. Bio Mater. 4, 7932 (2021).
- ²⁰M. Richardson, P. K. Das, S. Morrill, K. J. Suthar, S. K. R. S. Sankaranarayanan, and V. R. Bhethanabotla, "Removal of non-specifically bound proteins using Rayleigh waves generated on ST-Quartz substrates," Sensors 22, 4096 (2022).
- ²¹S. Cular, D. W. Branch, V. R. Bhethanabotla, G. D. Meyer, and H. G. Craighead, "Removal of nonspecifically bound proteins on microarrays using surface acoustic waves," IEEE Sens. J. 8, 314 (2008).
- ²²J. Friend and L. Y. Yeo, "Microscale acoustofluidics: Microfluidics driven via acoustics and ultrasonics," Rev. Mod. Phys. 83, 647 (2011).
- ²³W. L. Nyborg, "Acoustic streaming due to attenuated plane waves," J. Acoust. Soc. Am. 25, 68 (1953).
- ²⁴J. S. Bach and H. Bruus, "Theory of pressure acoustics with viscous boundary layers and streaming in curved elastic cavities," J. Acoust. Soc. Am. 144, 766 (2018).

- ²⁵R. M. Fand and J. Kaye, "Acoustic streaming near a heated cylinder," J. Acoust. Soc. Am. 32, 579 (1960).
- ²⁶G. Michel and G. P. Chini, "Strong wave-mean-flow coupling in baroclinic acoustic streaming," J. Fluid Mech. 858, 536 (2019).
- ²⁷M. Nabavi, K. Siddiqui, and J. Dargahi, "Influence of differentially heated horizontal walls on the streaming shape and velocity in a standing wave resonator," Int. Commun. Heat Mass Transfer 35, 1061 (2008).
- ²⁸W. Qiu, J. H. Joergensen, E. Corato, H. Bruus, and P. Augustsson, "Fast microscale acoustic streaming driven by a temperature-gradient-induced nondissipative acoustic body force," Phys. Rev. Lett. 127, 064501 (2021).
- ²⁹B.-G. Loh, S. Hyun, P. I. Ro, and C. Kleinstreuer, "Acoustic streaming induced by ultrasonic flexural vibrations and associated enhancement of convective heat transfer," J. Acoust. Soc. Am. 111, 875 (2002).
- 30 S. Hyun, D.-R. Lee, and B.-G. Loh, "Investigation of convective heat transfer augmentation using acoustic streaming generated by ultrasonic vibrations," Int. I. Heat Mass Transfer 48, 703 (2005).
- 31Y. Lin and B. Farouk, "Heat transfer in a rectangular chamber with differentially heated horizontal walls: Effects of a vibrating sidewall," Int. J. Heat Mass Transfer 51, 3179 (2008).
- ³²M. K. Aktas and T. Ozgumus, "The effects of acoustic streaming on thermal convection in an enclosure with differentially heated horizontal walls," Int. J. Heat Mass Transfer 53, 5289 (2010).
- 33P. D. Richardson, "Heat transfer from a circular cylinder by acoustic streaming," J. Fluid Mech. 30, 337 (1967).
- 34G. Michel and C. Gissinger, "Cooling by baroclinic acoustic streaming," Phys. Rev. Appl. 16, L051003 (2021).
- 35J. Kondoh, N. Shimizu, Y. Matsui, and S. Shiokawa, Liquid Heating Effects by SAW Streaming on the Piezoelectric Substrate (IEEE, 2005).
- ³⁶J. Kondoh, N. Shimizu, Y. Matsui, M. Sugimoto, and S. Shiokawa, Temperature-Control System for Small Droplet Using Surface Acoustic Wave Device (IEEE, Irvine, California, 2005).
- ³⁷J. Kondoh, N. Shimizu, Y. Matsui, M. Sugimoto, and S. Shiokawa, "Development of temperature-control system for liquid droplet using surface acoustic wave devices," Sens. Actuators A 149, 292 (2009).

- ³⁸S. Ito, M. Sugimoto, Y. Matsui, and J. Kondoh, "Study of surface acoustic wave streaming phenomenon based on temperature measurement and observation of streaming in liquids," Jpn. J. Appl. Phys. 46, 4718 (2007).
- ³⁹D. Beyssen, L. L. Brizoual, O. Elmazria, P. Alnot, I. Perry, and D. Maillet, 61-2 Droplet Heating System Based on Saw/Liquid Interaction (IEEE, 2006).
- ⁴⁰B. H. Ha, K. S. Lee, G. Destgeer, J. Park, J. S. Choung, J. H. Jung, J. H. Shin, and H. J. Sung, "Acoustothermal heating of polydimethylsiloxane microfluidic system," Sci. Rep. 5, 11851 (2015).
- ⁴¹N. Ohashin and J. Kondoh, "Temperature control of a droplet on disposable type microfluidic system based on a surface acoustic wave device for blood coagulation monitoring," in *IEEE International Ultrasonics Symposium*, *Taipei*, *Taiwan*, 2015 (IEEE, PIscataway, NJ, 2015), pp. 1–4.
- ⁴²J. Park, B. H. Ha, G. Destgeer, J. H. Jung, and H. J. Sung, "Spatiotemporally controllable acoustothermal heating and its application to disposable thermochromic displays," RSC Adv. 6, 33937 (2016).
- ⁴³P. K. Das, A. D. Snider, and V. R. Bhethanabotla, "Acoustothermal heating in surface acoustic wave driven microchannel flow," Phys. Fluids 31, 106106 (2019).
- 44Y. Wang, Q. Zhang, R. Tao, D. Chen, J. Xie, H. Torun, L. E. Dodd, J. Luo, C. Fu, J. Vernon, P. Canyelles-Pericas, R. Binns, and Y. Fu, "A rapid and controllable acoustothermal microheater using thin film surface acoustic waves," Sens. Actuators A 318, 112508 (2021).
- ⁴⁵T. Roux-Marchand, D. Beyssen, F. Sarry, and O. Elmazria, "Temperature uniformity of microdroplet heated by Rayleigh surface acoustic wave in view of biological reaction," in *IEEE International Ultrasonics Symposium*, *Prague*, *Czech Republic*, 2013 (IEEE, Piscataway, NJ, 2013), pp. 1885–1888.
- ⁴⁶H. Bruus, "Acoustofluidics 2: Perturbation theory and ultrasound resonance modes," Lab Chip 12, 20 (2012).
- ⁴⁷P. K. Das, A. D. Snider, and V. R. Bhethanabotla, "Acoustic streaming in second-order fluids," Phys. Fluids 32, 123103 (2020).
- ⁴⁸P. K. Das and V. R. Bhethanabotla, "Extra stress-mediated acoustic streaming in a surface acoustic wave driven microchannel filled with second-order fluids," Phys. Rev. Fluids 7, 074404 (2022).
- ⁴⁹C. P. Lee and T. G. Wang, "Near-boundary streaming around a small sphere due to two orthogonal standing waves," J. Acoust. Soc. Am. 85, 1081 (1989).